Ferromagnetism, superconductivity and quantum criticality in uranium intermetallics

Nguyen Thanh, H.

Publication date
2008

7. Coexistence of ferromagnetism and superconductivity in UCoGe

7.1. Introduction

Following the standard theory for superconductivity (SC) due to Bardeen, Schrieffer, and Cooper ferromagnetic (FM) order impedes the pairing of electrons in singlet states [155]. It has been argued, however, that on the borderline of ferromagnetism, critical magnetic fluctuations could mediate SC by pairing the electrons in triplet states [105]. The discovery several years ago of SC in the metallic ferromagnets UGe_2 (at high pressure) [34], URhGe [36], and possibly UIr (at high pressure) [37], has put this idea on firm footing. However, later work provided evidence for a more intricate scenario in which SC in UGe_2 and URhGe is driven by a magnetic transition between two polarized phases [38,86,110] rather than by critical fluctuations associated with the zero temperature transition from a paramagnetic to a FM phase.

Within a search for a FM QCP in polycrystalline $URh_{1-x}Co_xGe$ alloys with x in the range $0 \leq x \leq 1$ (as reported in Chapter 6), we found a new ferromagnetic superconductor: the end compound UCoGe. In this chapter, we report our discovery that was made by carefully investigating the magnetic, transport, thermal and microscopic properties on both poly- and single-crystalline UCoGe.

The experiments on polycrystalline UCoGe provide solid evidence for the coexistence of bulk magnetism and superconductivity at ambient pressure. The data show that UCoGe is a weak itinerant ferromagnet with a Curie temperature $T_C = 3$ K and a small ordered moment

$m_0 = 0.03\ \mu_B$, while SC is observed with a resistive transition temperature $T_S = 0.8$ K for the best sample.

Subsequent experiments on single crystalline UCoGe reveal the anisotropy in the magnetic and superconducting properties. Magnetization data show that UCoGe is a uniaxial FM, with an ordered moment $m_0 = 0.06\ \mu_B$ pointing along the orthorhombic c axis. The upper critical field $B_{c2}(T)$ is obtained by resistivity measurements for B applied along the orthorhombic axes. For the field along the a and b axes, $B_{c2}(T)$ is not Pauli limited and exhibits a large anisotropy. The single crystal data reveal UCoGe is a triplet superconductor with equal-spin pairing state, and a SC gap function of axial symmetry with point nodes along the direction of the ordered moment. Furthermore, a pronounced positive curvature or kink is observed in $B_{c2}(T)$ which possibly indicates two-band superconductivity.

Since SC occurs right on the borderline of FM order (and not near a transition between two polarized phases as for UGe_2 and URhGe), UCoGe may present the first example of triplet SC stimulated by critical fluctuations associated with a FM quantum critical point (QCP).

7.2. Polycrystalline UCoGe

7.2.1. Sample preparation and characterization

Several batches of polycrystalline UCoGe samples were prepared and characterized as described below.

The first polycrystalline UCoGe batches (samples #1 and #2) were prepared with nominal composition $U_{1.02}CoGe$ by arc-melting the constituents U, Co (both 3N purity) and Ge (5N purity) under a high-purity argon atmosphere. The as-cast samples were annealed for 10 days at 875 ^{o}C. The EPMA analysis of the annealed samples shows that 98% of the sample volume consists of the matrix UCoGe, and that the samples contained small amounts (2%) of impurity phases. The secondary phases are Uranium rich phases with main nominal composition U_5Ge_3 and U_5Ge_4 for sample #1 and #2, respectively. The EPMA micrograph of sample #1 is shown in the right panel of Fig. 6.5. The residual resistance ratio $RRR = \rho(300\ K)/\rho(1\ K)$, which characterizes the quality of the samples, is ~ 10. (Notice, the magnetization and transport properties of polycrystalline UCoGe reported in Chapter 6 were measured on sample #1).

In order to improve the quality of the samples further, we added 2% of Co to the starting materials to prevent formation of the secondary phases (U_5Ge_3 and U_5Ge_4).

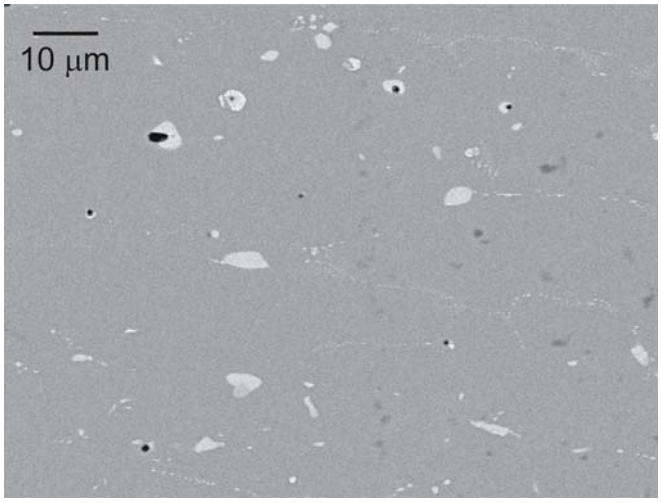

Figure 7.1 EPMA micrograph of UCoGe (sample #3). The grey area represents the main matrix UCoGe. The (big and small) light spots are Uranium rich phases, while the dark grey spots are Uranium poor phases. The black spots are holes on the surface.

A polycrystalline UCoGe batch (sample #3) was prepared with nominal composition $U_{1.02}Co_{1.02}Ge$. The as-cast sample was annealed for 10 days at 875 ^{o}C. EPMA measurements on the annealed sample show that the main matrix again comprises 98% of the sample, and that small amounts (~ 2%) of impurity phases are still present, see Fig. 7.1. The impurity phases now consist of different solid solutions of U, Co and Ge with main nominal compositions of a light phase U:Co:Ge 4:1:1 (light spots) and a dark phase U:Co:Ge 1:2:1.3 (dark grey spots). But most importantly, the quality of the sample has significantly improved. The *RRR* value has increased up to 27. Also, subsequent batches #4 and #5 with nominal compositions $U_{1.02}Co_{1.02}Ge$ all have *RRR*'s of ~ 30.

X-ray diffraction patterns taken on powdered samples confirm UCoGe has the TiNiSi structure and the lattice parameters extracted are a = 6.845 Å, b = 4.206 Å and c = 7.222 Å, in agreement with literature data [151].

7.2.2. Magnetization

The temperature variation of the magnetization of polycrystalline UCoGe measured in a field of 0.01 T is shown in Fig. 7.2. The curves taken on samples prepared from different batches, *e.g.* samples #2 and #3, almost coincide. The demagnetizing factor of our samples

is small ($N \approx 0.08$) and corrections due to the demagnetizing field were neglected. The Curie temperature T_C = 3 K is deduced from the temperature derivative of the magnetization and from the Arrott plot (see Fig. 6.7 and Fig. 6.8 in Section 6.3.2). A hysteresis loop with a coercive field of 0.3 mT measured at 2 K further corroborates FM order, see the inset of Fig. 7.2. The very small size of the ordered moment of 0.03 μ_B and the very large ratio of p_{eff}/M_S (see Table 6.3) classify UCoGe as a weak itinerant ferromagnet [82,132].

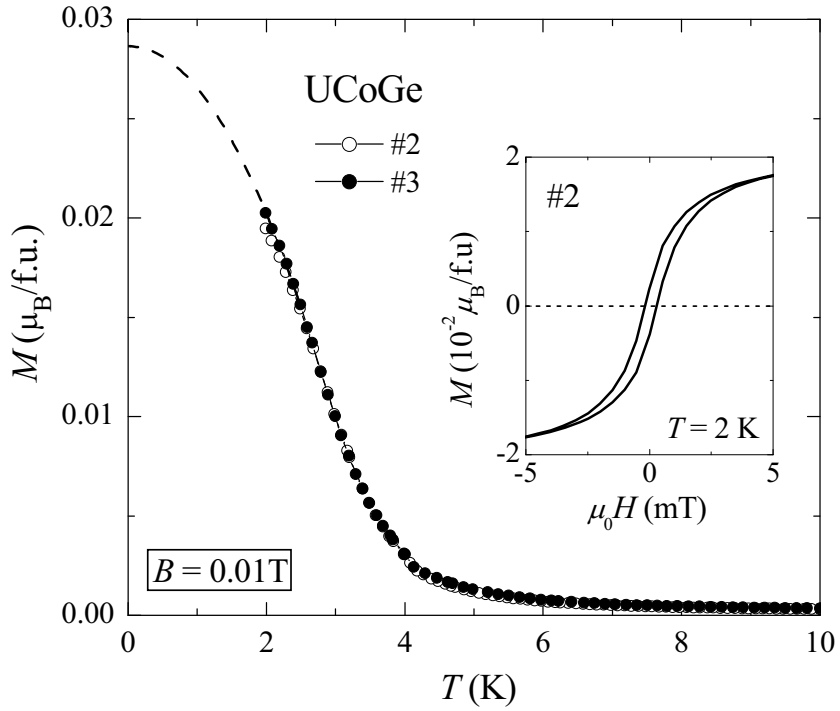

Figure 7.2 Magnetization of UCoGe (samples #2 and #3) as a function of temperature in a field B of 0.01 T as indicated. The dashed line is a smooth extrapolation of the data for sample #3 to 0 K. *Inset*: Hysteresis loop measured for sample #2 at 2 K in the FM state.

7.2.3. Electrical resistivity

In Fig. 7.3, the temperature dependence of the electrical resistivity of UCoGe samples is shown for $T < 10$ K. Notice that samples #1, #2 have $RRR \approx 10$ and samples #3 - #5 have $RRR \approx 30$. A broad hump around 3 K associated with the ferromagnetic transition is observed for all samples. Upon further cooling, superconductivity is found with resistive onset temperatures of ~ 0.6 K and ~ 0.8 K for samples with RRR's of 10 and 30, respectively. The magnetic transition is a robust property of our polycrystalline samples, but the superconducting properties depend sensitively on the quality of the samples as determined by the RRR. The superconducting transition is relatively broad ($\Delta T_S \approx 0.15$ K),

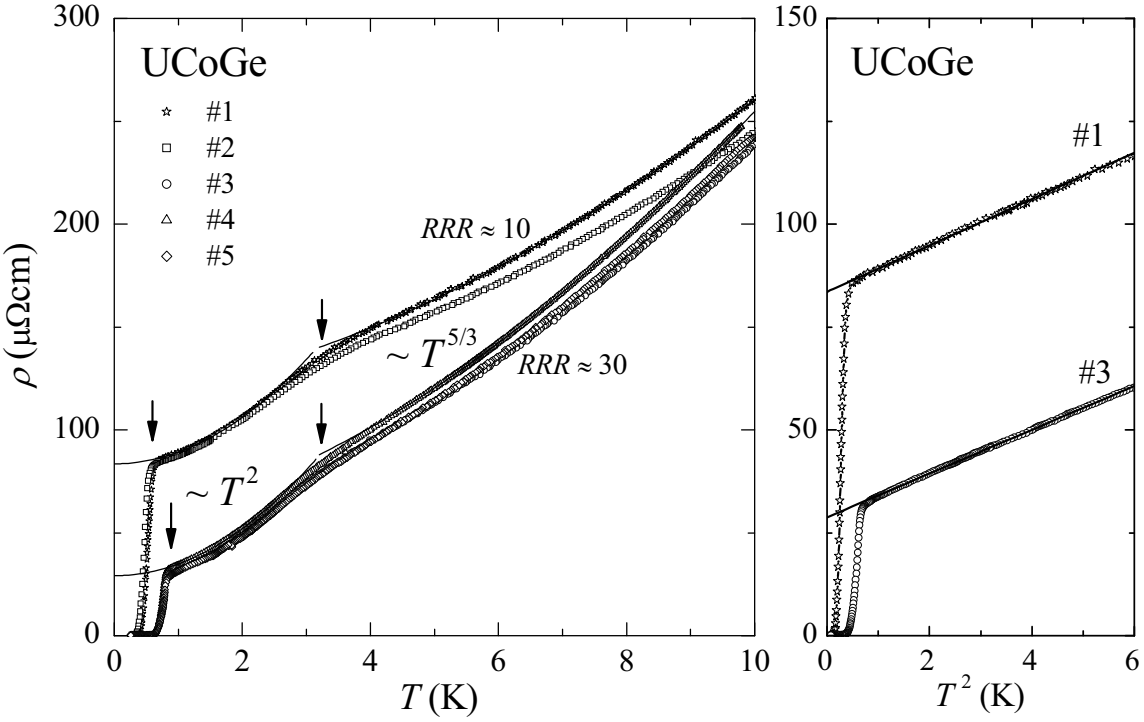

Figure 7.3 Left frame: Temperature dependence of the electrical resistivity measured on polycrystalline UCoGe samples (from top to bottom: #1, #2 ($RRR \approx 10$), #3 - #5 ($RRR \approx 30$)). Arrows indicate the Curie temperature T_C and superconducting transition temperature T_S. The solid lines represent fits of the data for samples #1 and #3 to $\rho \sim T^2$ and $T^{5/3}$ in the temperature ranges below and above T_C, respectively. *Right frame*: The resistivity of UCoGe plotted versus T^2. The solid lines represent the fits of data to $\rho \sim T^2$.

where T_S is the superconducting transition temperature which is defined at the mid-point of the resistivity drop.

In the FM phase ($T_S < T < 0.8T_C$), the resistivity obeys the relation $\rho = \rho_0 + AT^2$, as shown in the right frame of Fig. 7.3 for samples #1 and #3. The values of the coefficient A are almost equal, 5.5 ± 0.2 μΩcm/K^2, whereas the residual resistivity ρ_0 obtained by extrapolating the $\rho(T)$ curves to 0 K are 28.8 and 83.5 μΩcm for samples #1 and #3, respectively. In the temperature range $T_C \lesssim T \lesssim 3T_C$ the resistivity is well described by a function $\rho \sim T^{5/3}$. The temperature dependence of the resistivity of UCoGe ($\sim T^2$ and $T^{5/3}$ for T below and above T_C, respectively) is characteristic for a weak itinerant electron ferromagnet (see for instance the data for $ZrZn_2$ [156] and Sc_3In [157]). The T^2 term below T_C is due to scattering at magnons, while for $T > T_C$ the $T^{5/3}$ term signals scattering at critical FM spin fluctuations. Here the $T^{5/3}$ term results from a calculation based on the self consistent renormalization (SCR) theory for a 3D critical ferromagnet [82,158]. The

resistivity data provide further evidence that UCoGe is near the critical boundary for magnetic long-range order.

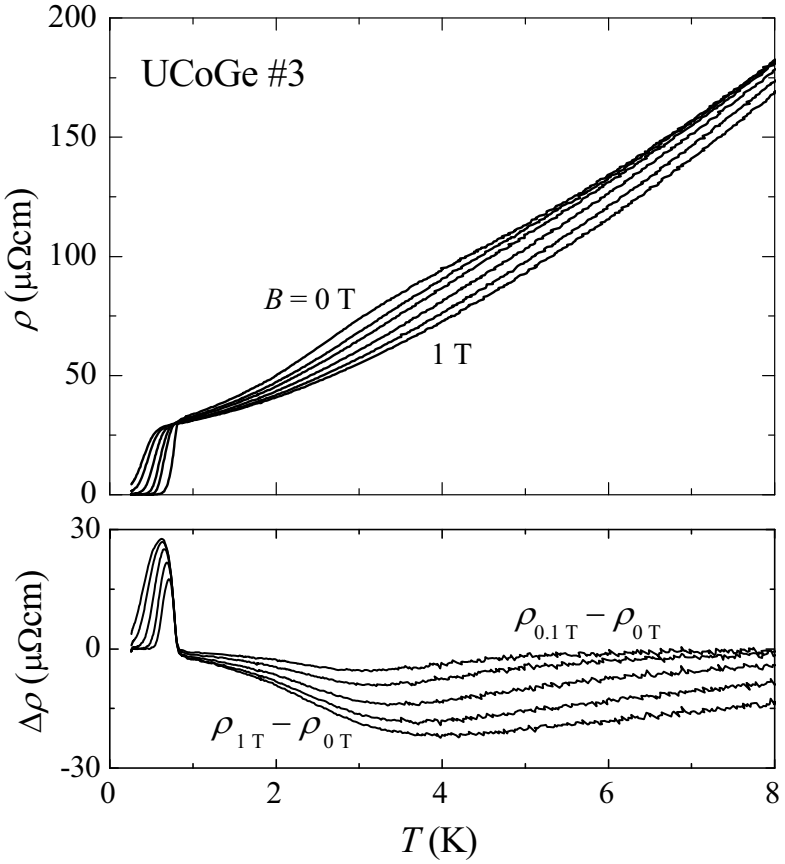

Figure 7.4 The temperature dependence of the resistivity of polycrystalline UCoGe (sample #3) in applied fields of 0, 0.1, 0.2, 0.4, 0.7 and 1 T (*upper frame*) and $\Delta\rho$ obtained by subtracting of the zero-field resistivity from the resistivity measured in applied field (*lower frame*).

The temperature dependence of the resistivity of UCoGe (sample #3) measured in zero and applied fields up to 1 T is shown in Fig. 7.4. The broad hump, due to ferromagnetic ordering, becomes less pronounced and is completely washed out at 1 T. Upon increasing the magnetic field, the hump shifts to higher temperatures. This is most clearly observed in the lower frame of Fig. 7.4, where we subtracted the zero field data from the data measured in field. A negative magnetoresistance result, which exhibits a large enhancement near T_C in magnetic field. These phenomena are well described by the SCR theory [159], in which spin fluctuations in weak itinerant electron magnets, such as $ZrZn_2$ [82], Sc_3In [157], Ni_3Al [160], are suppressed by a magnetic field, giving rise to a negative magnetoresistance.

The superconducting state observed below 1 K is suppressed in a magnetic field. The data are further shown in Fig. 7.11 when the upper critical field in polycrystalline UCoGe

is presented, see Section 7.2.7.

7.2.4. ac-susceptibility

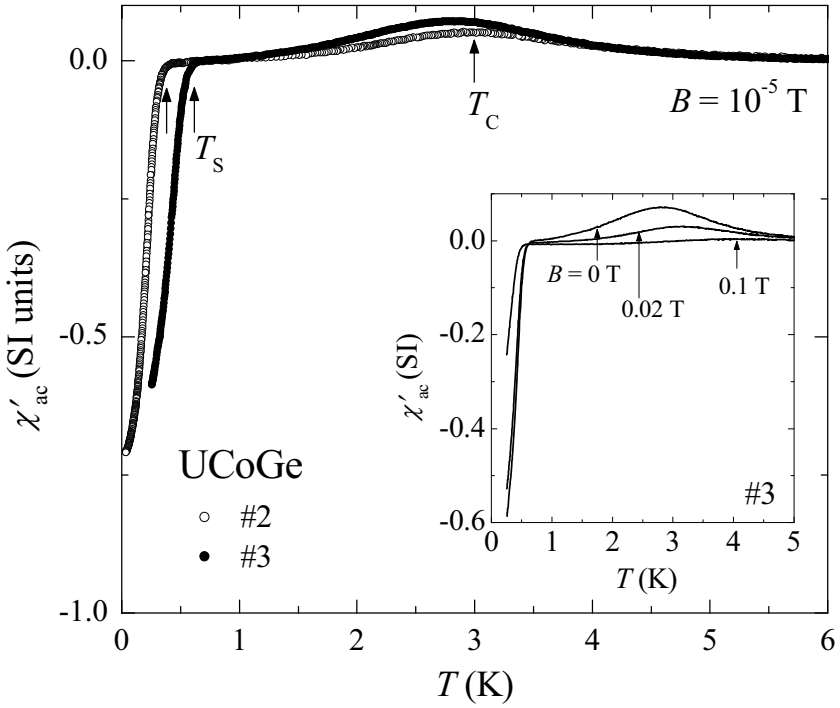

Figure 7.5 Temperature dependence of the real part of the ac-susceptibility χ'_{ac} in polycrystalline UCoGe (samples #2 and #3). Arrows indicate T_C and T_S. *Inset*: The ac-susceptibility of sample #3 measured in fields of 0, 0.02 and 0.1 T.

Ac-susceptibility measurements are carried out at a low frequency of 16 Hz and in a small driving field of ~ 10^{-5} T. Fig. 7.5 shows the real part of the ac-susceptibility, χ'_{ac}, of polycrystalline UCoGe (samples #2 and #3) as a function of temperature. The weak peak observed at 3 K reveals the ferromagnetic transition. Below 1 K, χ'_{ac} rapidly decreases to a large diamagnetic value, which reflects the superconducting transition. The onset transition temperatures $T_{S,onset}$ are determined at 0.38 and 0.61 K for samples #2 ($RRR \approx 10$) and #3 ($RRR \approx 30$), respectively. Clearly, superconductivity depends sensitively on the quality of the samples. These results are in good agreement with the resistivity data. However, the ac-susceptibility χ'_{ac} starts to drop when the resistive transition is complete. At the lowest temperature χ'_{ac} reaches a value of 60 - 70% of the ideal screening value $\chi_S = -1/(1 - N)$ (here $N \approx 0.08$ is the demagnetizing factor of our samples). This indicates UCoGe is a type II SC which is always in the mixed phase. A similar observation [36] with a comparable screening fraction was made for URhGe. Because of the intrinsic FM moments the local

field is nonzero and the magnitude of χ'_{ac} is reduced.

The temperature dependence of the ac-susceptibility of sample #3 for various magnetic fields is shown in the inset of Fig. 7.5. In an applied field, the peak associated with the ferromagnetic order broadens and shifts to higher temperatures, while the onset temperature for superconductivity shifts to lower temperatures. This is in accordance with the resistivity data. In a field of 0.1 T, the magnetic transition is almost washed out, much faster than in the resistivity data.

7.2.5. Specific heat

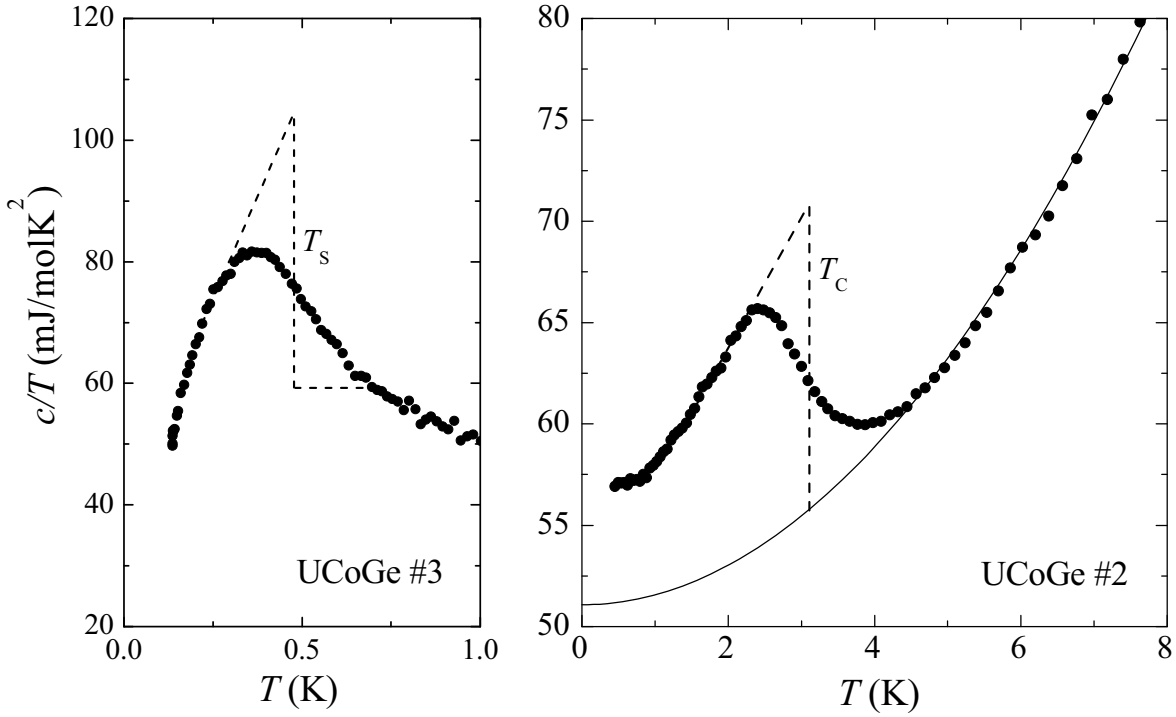

Figure 7.6 Temperature dependence of the specific heat of UCoGe divided by temperature c/T in zero field. The solid line represents an estimate of the lattice contribution together with an electronic term of 50.4 mJ/molK^2. *Left panel*: c/T in the temperature range 0.1 - 1 K measured on sample #3. *Right panel*: c/T in $T > 0.5$ K measured on sample #2.

In Fig. 7.6, we show the temperature dependence of the specific heat of UCoGe measured in zero field. The right panel shows c/T versus T of sample #2 measured in the Van der Waals - Zeeman institute in a specific heat set-up employing an adiabatic method down to 0.5 K. The FM transition results in a broad peak and the Curie temperature T_C = 3 K is identified by the inflection point in c/T at the high T side of the peak. T_C determined in this way agrees well with T_C determined by the magnetization and transport data.

The lattice contribution to the specific heat, $c_{lat} = \beta T^3$, is estimated by fitting the data in the temperature range 4 K < T < 10 K. We obtain $\beta = 0.54\times10^{-3}$ J/molK^4, which gives a Debye temperature θ_D of 220 K (Eq. 4.6). The linear term in the electronic specific heat amounts to 0.057 J/molK^2, which indicates UCoGe is a correlated metal, but the electron interactions are relatively weak. The magnetic entropy S_{mag} involved in the magnetic transition by integrating c_{mag}/T versus T is 0.3% of Rln2 (*i.e.* the value for a local moment S = ½ system). Such a small value is expected for a weak itinerant ferromagnet [161].

As mentioned, $T_{S,onset}$ as determined by the ac-susceptibility equals 0.38 and 0.61 K for samples #2 and #3, respectively. Consequently, we cannot probe the SC transition with our in-house specific heat set-up which has a low temperature limit of 0.5 K. Low temperature specific heat data (0.1 - 1 K) have been measured in a dilution refrigerator at the University of Karlsruhe (in collaboration with the group of Prof. H. von Löhneysen) using a compensated heat loss method.

In the left panel of Fig. 7.6 we show the zero-field specific heat plotted as c/T versus T of sample #3 in the temperature range 0.1- 1 K. The data show a broad superconducting transition with an onset temperature of 0.66 K, which is almost equal to the temperature at which the resistance becomes zero. A rough estimate for the step size of the idealized transition (dashed line in Fig. 7.6) in the specific heat using an equal entropy construction (at $T_S \approx 0.45$ K) is $\Delta(c/T_S)/\gamma \approx 1.0$, which is smaller than for a conventional SC (the BCS value is 1.43) [32] but comparable to the value for URhGe [36].

The temperature variation of the specific heat divided by temperature c/T of UCoGe (sample #2) measured in fields up to 0.3 T in the temperature range 0.5 - 6 K is presented in Fig. 7.7. The analysis of data shows that the magnetic entropy S_{mag} of 0.3% of Rln2 is constant and independent of the magnetic field. The linear term in the electronic specific heat γ slightly decreases with increasing magnetic field. The anomaly around T_C associated with the FM transition is significantly smeared out and shifts to higher temperatures. A similar variation of c/T versus T near T_C in fields has been observed in URhGe [119], and is probably related to the strong magneto-crystalline anisotropy (UCoGe is a uniaxial ferromagnet with an ordered moment pointing along the orthorhombic c-axis, see Section 7.3.2). Additionally, the field dependence of the specific heat in UCoGe can be discussed in terms of the quenching of spin fluctuations. Theoretical studies for weak

itinerant ferromagnets predict that the magnetic contribution to the specific heat of compounds, like Sc_3In [162], is governed by spin fluctuations [163], which may be quenched in a large magnetic fields [164]. As a result, the peak near T_C becomes less pronounced and shifts to higher temperatures.

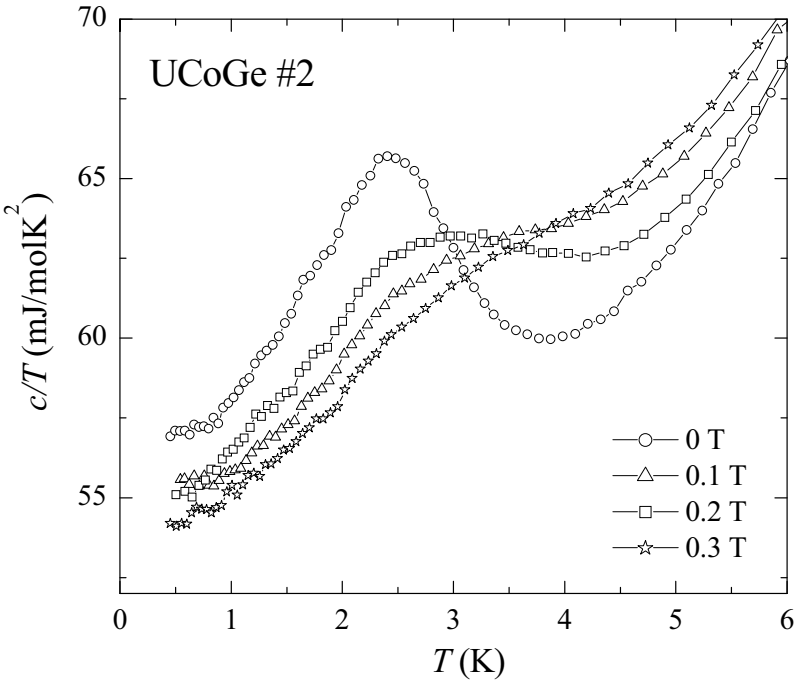

Figure 7.7 The temperature dependence of the specific heat of UCoGe (sample #2) plotted as c/T versus T in fields of 0, 0.1, 0.2 and 0.3 T.

7.2.6. Muon spin relaxation and rotation

In order to investigate the weak itinerant ferromagnetism of UCoGe on a microscopic scale we have carried out muon spin relaxation and muon spin rotation experiments. In the μSR technique the muon is employed as an extremely sensitive probe for magnetic signals [54,55]. The main objectives of our experiments were twofold: (i) to investigate whether weak ferromagnetism is a bulk property of our samples, and (ii) to provide hard proof for the coexistence of ferromagnetism and superconductivity. As regards the first objective, one should realize that the magnetization data, as measured with the squid technique, and the specific heat data cannot exclude that the weak magnetic signal and the small value of the magnetic entropy are due to a small amount of a secondary phase (2%) which orders ferromagnetically with a large moment of ~ 1.5 μ_B. Since the muon localizes at an interstitial site, it probes the local field and it therefore allows one to discern magnetically inequivalent sample regions. Consequently, μSR is an excellent technique to probe the bulk

nature of weak ferromagnetism. As regards the second objective, the ac-susceptibility and specific heat data cannot completely exclude that ferromagnetism is (partially) expelled from the sample when superconductivity sets in. It is therefore of paramount importance to follow the ferromagnetic signal to deep in the superconducting state by the μSR technique.

A new batch (#4) of polycrystalline UCoGe was prepared and subsequently annealed. The *RRR* value amounts to 30 and the ferromagnetic and superconducting transitions occur around 3.0 K and 0.7 K, respectively (see Fig. 7.3). Zero-field (ZF) μSR experiments were performed at the Paul Scherrer Institute (Villigen). Data were collected in the General Purpose Spectrometer (GPS) in the temperature range 1.6 - 10 K and in the Low Temperature Facility (LTF) in the temperature range 0.02 - 5.5 K. In order to measure in the GPS and LTF simultaneously, we prepared two μSR samples taken from the same UCoGe batch. In order to compare the weak magnetic signal of UCoGe with that of a doped sample with pronounced magnetic order, we carried out, in addition, ZF μSR experiments on polycrystalline $URh_{0.4}Co_{0.6}Ge$, which has a Curie temperature T_C = 19.9 K and an ordered moment m_0 = 0.22 μ_B/f.u. (see Chapter 6).

In the paramagnetic state the muon depolarization $P(t)$ of UCoGe in ZF is best described by the standard Kubo-Toyabe function [165]:

$$P_{KT}(t) = \frac{1}{3} + \frac{2}{3}(1 - \Delta_{KT}{}^2 t^2)\exp(-\frac{1}{2}\Delta_{KT}{}^2 t^2) \qquad (7.1)$$

Here $\Delta_{KT} = \gamma_\mu \sqrt{< B^2 >}$ is the Kubo-Toyabe relaxation rate, with γ_μ the muon gyromagnetic ratio ($\gamma_\mu/2\pi$ = 135.5 MHz/T) and $<B^2>$ the second moment of the field distribution at the muon site. The Kubo-Toyabe function describes the case of an isotropic Gaussian distribution of static internal fields centered at zero field. A typical spectrum taken in the GPS at T = 5.5 K is shown in the upper panel of Fig. 7.8. The best fit using Eq. 7.1 is obtained for a Kubo-Toyabe relaxation rate Δ_{KT} = 0.298 ± 0.003 μs^{-1}. Spectra taken in the paramagnetic regime show Δ_{KT} is independent of temperature, which suggests the depolarization is due to a static distribution of cobalt nuclear moments (I = 7/2, μ_{Co} = 5.23 μ_N, abundancy 1).

At low temperatures, in the ferromagnetic state, the spectra show a spontaneous μ^+ precession frequency ν and are dominated by the depolarization signal of an isotropic polycrystalline magnet with a Lorentzian field distribution:

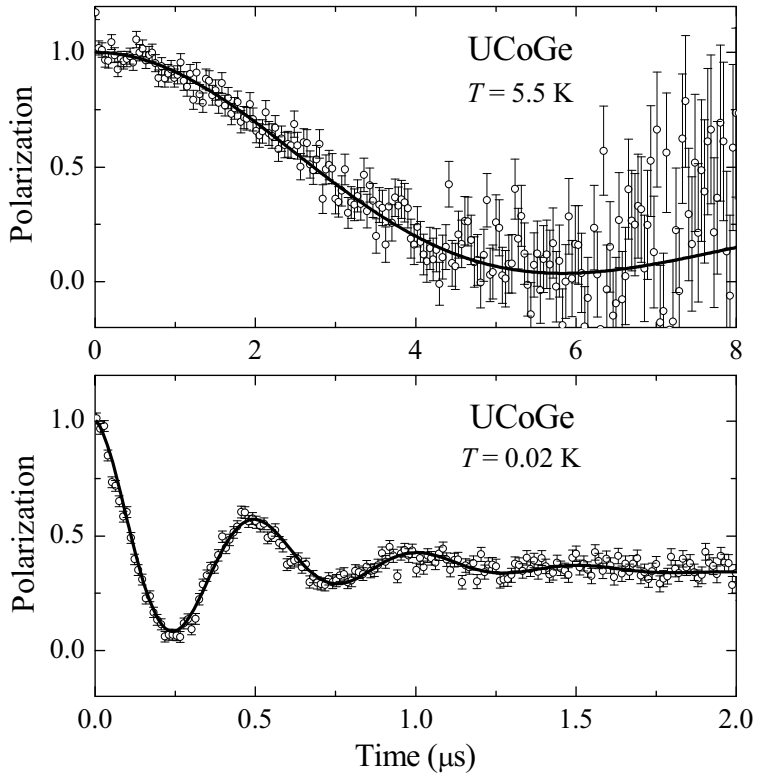

Figure 7.8 Time dependence of normalized muon spin polarization of the polycrystalline compound UCoGe in zero magnetic field (*upper panel*) in the paramagnetic phase, at 5.5 K, and (*lower panel*) in the ferromagnetic phase, at 0.02 K. The solid lines represent fits of Eq. 7.1 and Eq. 7.2 to the data taken at 5.5 K and 0.02 K. Notice the horizontal scales are different.

$$P_M(t) = \frac{1}{3}\exp(-\lambda_1 t) + \frac{2}{3}\exp(-\lambda_2 t)\cos(2\pi\nu\, t + \phi) \tag{7.2}$$

The "⅓ term" is due to the component of the ordered moment parallel to the initial muon spin direction, while the "⅔ term" is due to the orthogonal components, which give rise to a precession of the muon spin with frequency ν (here ϕ is a phase factor). Best fits were obtained using exponential damping factors, $\exp(-\lambda_1 t)$ and $\exp(-\lambda_2 t)$. In the lower panel of Fig. 7.8 we show a typical spectrum taken in the LTF at a very low temperature $T = 0.02$ K. The spontaneous muon precession frequency $\nu = 1.953 \pm 0.004$ MHz, and the damping rates are $\lambda_1 = 0.157 \pm 0.006$ μs^{-1} and $\lambda_2 = 2.399 \pm 0.035$ μs^{-1}. In all LTF spectra a small fraction of the signal (13% of the full asymmetry) is due to muons that localize in the silver sample holder (the UCoGe sample does not completely cover the silver sample support). This background signal was determined by fitting the high-temperature LTF spectra (at 5 K) with two Kubo-Toyabe contributions. One with $\Delta_{KT} = 0.298 \pm 0.003$ μs^{-1} due to the

cobalt nuclear moments and the background contribution with a fixed small value $\Delta_{KT} = 0.01\ \mu s^{-1}$ due to silver nuclear moments.

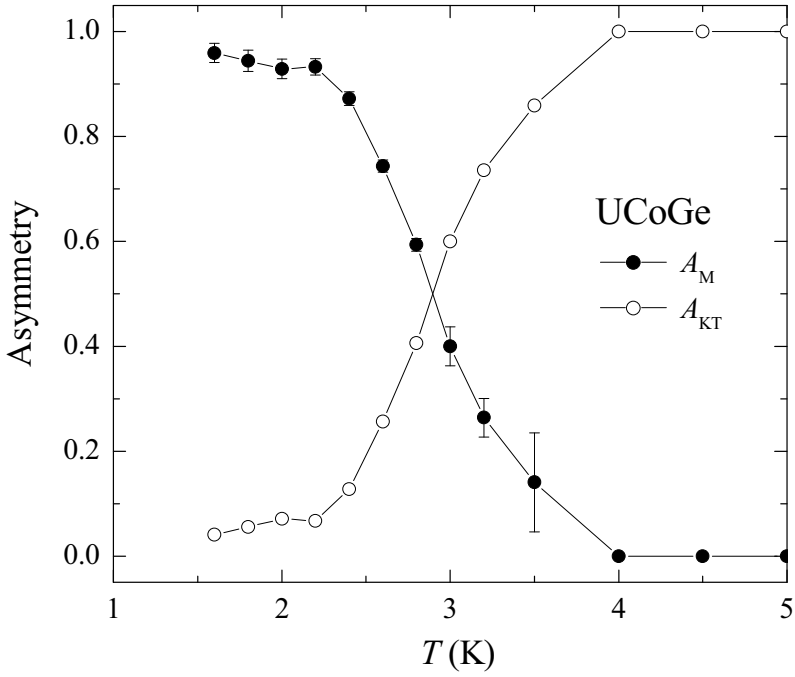

Figure 7.9 The temperature dependence of the asymmetries (signal amplitudes), A_M and A_{KT}, determined by fitting the data to Eq. 7.3.

In the intermediate temperature regime, *i.e.* in the range of the ferromagnetic transition, the GPS spectra are best described by the sum of the limiting depolarization functions:

$$P(t) = A_M P_M(t) + A_{KT} P_{KT}(t) \tag{7.3}$$

with the normalization $A_M + A_{KT} = 1$ (notice for the LTF spectra one has to add the small contribution from the silver holder as a third term). In Fig. 7.9 we show the temperature variation of A_M and A_{KT} determined in this way, which confirms the magnetic transition in these polycrystalline samples is relatively broad. The un-renormalized asymmetry is almost equal to the value obtained at T = 10 K in transverse field geometry (TF = 50 G). This shows ferromagnetic order is found in the whole sample volume.

The temperature variation $\nu(T)$ as deduced from the LTF spectra is shown in Fig. 7.10 and tracks the macroscopic magnetization $M(T)$. For $T \leq T_C$, the data are well described by the relation

$$\nu(T) = \nu_0 (1 - (T/T^*)^\alpha)^\beta \tag{7.4}$$

By fitting the data to Eq. 7.4, we obtain values of the spontaneous frequency $\nu_0 = 1.98$ MHz

for $T \rightarrow 0$, the critical temperature $T^* = 3.02$ K $\simeq T_C$, $\alpha = 2.3$, and the critical value $\beta = 0.4$ which is close the theoretical value predicted for 3D Ising-like magnet. The frequency $\nu \simeq \nu_0 = 2$ MHz measured at low temperatures, corresponds to an internal field $B_i \sim 0.0148$ T at the muon localization site. These data provide unambiguous proof for magnetic order being present in the whole sample volume. Moreover, magnetic order persists in the superconducting state. Interestingly, in the superconducting state the precession frequency shows a small decrease of about 2%, indicating magnetism and superconductivity interact.

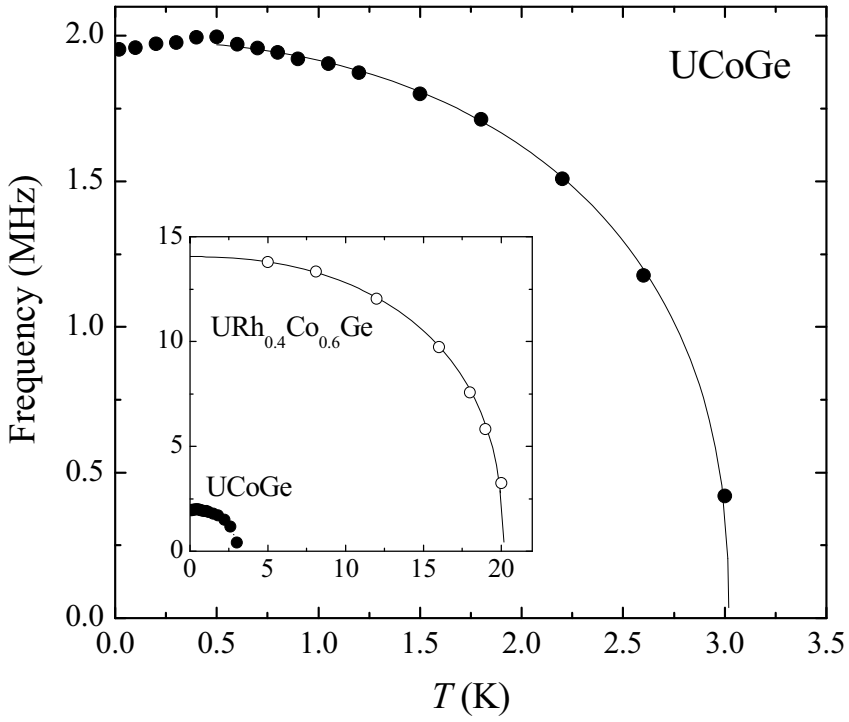

Figure 7.10 Temperature dependence of the muon precession frequency $\nu(T)$ of the polycrystalline sample UCoGe in zero magnetic field. *Inset*: The $\nu(T)$ curve of the polycrystalline sample $URh_{0.4}Co_{0.6}Ge$ in zero field. The solid lines represent fits of the data to Eq. 7.4.

The ZF μSR spectra measured on the doped sample $URh_{0.4}Co_{0.6}Ge$ in the GPS in the temperature range 5 - 25 K further corroborate the analysis for pure UCoGe. Using a similar analysis, we obtain the temperature variation $\nu(T)$ of the compound $URh_{0.4}Co_{0.6}Ge$, as shown in the inset of Fig. 7.10. Using the 3D Ising-like model (Eq. 7.4) to fit the $\nu(T)$ data for $URh_{0.4}Co_{0.6}Ge$ we obtain $T^* = 20.1$ K $\simeq T_C$, $\nu_0 = 14.05$, $\alpha = 2.2$ and $\beta = 0.4$. The values for α and β are similar to the ones derived from the magnetization data (see Section 6.3.2). The frequency at low temperatures is a factor ~ 7 larger than the one of UCoGe, in agreement with the ratio of the ordered moments (~ 7.5) as deduced from the dc-

magnetization measurements (see Table 6.3).

In summary, the μSR data on polycrystalline UCoGe provide unambiguous evidence for bulk ferromagnetism, which coexists with superconductivity. The μSR spectra at low temperatures are adequately described by the depolarization function for a polycrystalline magnet. Our analysis indicates that muons localize at one single stopping site. This may be further corroborated by calculating the local field (experimental value $B_i \sim 0.0148$ T) due to the electronic and nuclear dipolar moments for different interstitial sites, as well as by calculations of the dipolar tensor $\boldsymbol{A}_{dip}$ in combination with Knight shift experiments on a single-crystalline sample (see *e.g.* Ref.[54]). As regards the superconducting state, it will be highly interesting to investigate the inhomogeneous field distribution due to the flux line lattice, in order to extract the penetration depth. Preliminary experiments in the LTF on our polycrystalline samples show, however, that the μSR spectra are dominated by the relatively large internal field $B_i \sim 0.015$ T due to ferromagnetism. Experiments on single-crystalline samples are required in order to shed more light on this issue.

7.2.7. Upper critical field B_{c2}

By studying the temperature dependence of the upper critical field, $B_{c2}(T)$, we obtain important information about the nature of the SC state. Normally, the upper critical field is obtained from the resistively measured superconducting transition curves. Here we use a simple model to analyse the upper critical field. It is based on Ginzburg-Landau theory for type-II superconductors, and under the very crude assumption of a spherical Fermi surface, has been applied to A15 compounds [166] and heavy fermion systems [167]. The analysis of $B_{c2}(T)$ yields microscopic parameters of the SC state (*i.e.* the coherent length ξ) and the normal state (*i.e.* the mean free path ℓ), using the relation

$$B'_{c2} = -\frac{\partial B_{c2}}{\partial T}\Big|_{T_S} = R(\ell)\left(1.18\times10^{35}\,\frac{\gamma^2 T_S}{S_S^2} + 4490\gamma\rho_0\right) \tag{7.5}$$

where S_S is that part of the Fermi surfaces, on which Cooper pairs are formed; $R(\ell)$ is a parameter which varies between $R = 1$ in the dirty and $R = 1.17$ in the clean limit; γ is the linear term in the electronic molar specific heat. Notice that all parameters are in SI units. In the clean limit (ρ_0 small, $\ell \gg \xi$) the first term mainly contributes to B'_{c2}. Whereas, in the dirty limit (ρ_0 large, $\ell \ll \xi$) B'_{c2} is determined by the second term. Subsequently, the

microscopic parameters (*i.e.* ℓ, ξ) can be calculated as below, where the quantities a and b are give by 1.533×10^{6} Ω and 6.61×10^{-26} J/K

$$\ell = a\frac{1}{\rho_0 S_S} \tag{7.6}$$

$$\xi = b\frac{S_S}{\gamma T_S} \tag{7.7}$$

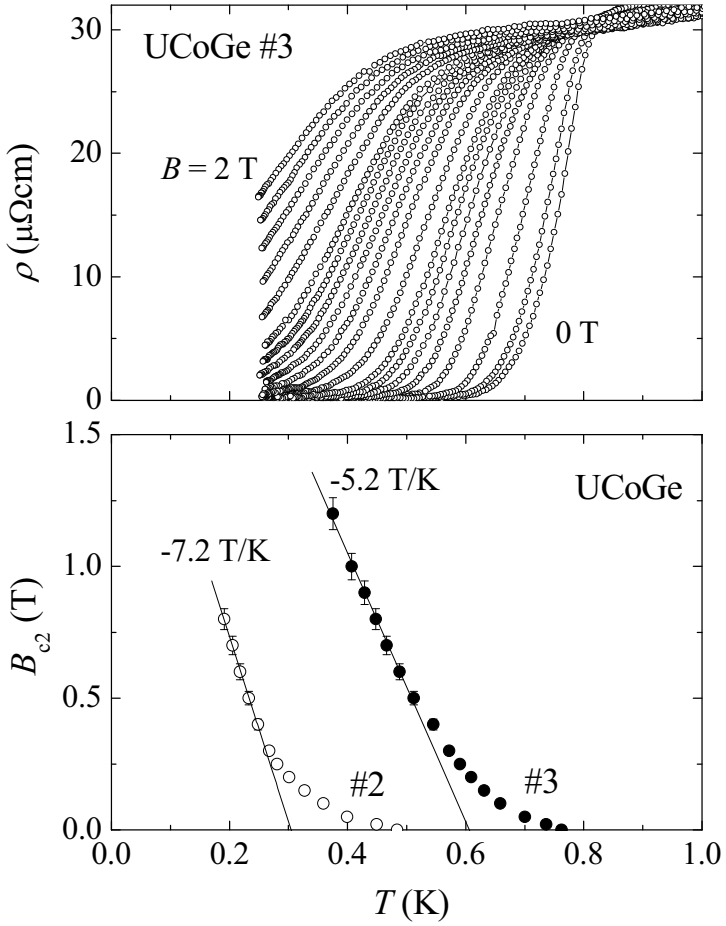

Figure 7.11 Upper frame: Resistive superconducting transition of UCoGe (sample #3) measured in magnetic fields (from right to left) of 0, 0.02, 0.05, 0.1, 0.15, 0.2, 0.25, 0.3, 0.4, 0.5, 0.6, 0.7, 0.8, 0.9, 1.0, 1.2, 1.4, 1.6, 1.8 and 2.0 T. *Lower frame*: Upper critical field (B_{c2}) of polycrystalline UCoGe determined by the midpoints of the resistive transitions measured in fixed magnetic fields. The solid lines indicate a quasi-linear behaviour of B_{c2} with dB_{c2}/dT = -7.2 T/K and -5.2 T/K for samples #2 and #3, respectively, and extrapolate to superconducting transitions in zero field at 0.30 K and 0.60 K.

In Fig. 7.11, the temperature dependence of the upper critical field (B_{c2}) for samples #2 and #3 is shown. The curvature (or tail) of B_{c2} is attributed to sample inhomogeneities and anisotropy. The quasi-linear behavior of $B_{c2}(T)$ at high fields extrapolates to

superconducting transitions in zero field at 0.30 K and 0.60 K. These values are close to the onset temperatures of the diamagnetic signal. From the slope of the upper critical field dB_{c2}/dT (near T_S) and the values of γ and ρ_0, we can make a crude estimate using Eq. 7.6 and Eq. 7.7 for the coherence length ξ and the mean free path ℓ. For sample #3, dB_{c2}/dT = -5.2 T/K and the measured ρ_0 = 28.8 μΩcm and we calculate $\xi \approx \ell \approx 200$ Å. However, as cracks in the polycrystalline samples affect the absolute resistivity values (see section 2.4) we normalize the resistivity value at 300 K by the value obtained for single crystalline UCoGe: ρ(300 K) ≃ 300 μΩcm (see Section 7.3). With *RRR* = 27 we then obtain ρ_0 = 12 μΩcm and calculate $\xi \approx 150$ Å and $\ell \approx 500$ Å. This indicates sample #3 satisfies the clean-limit condition ($\ell > \xi$), a prerequisite for unconventional SC [168]. For the less pure sample #2 we find $\xi \approx 200$ Å and $\ell \approx 300$ Å. The value of the upper critical field at low temperatures exceeds the BCS Pauli paramagnetic limit [166,169] ($B_{c2,Pauli} = 1.83 T_S \approx 1$ T for sample #3), which for spin-singlet pairing is only possible in the case of strong spin-orbit scattering. On the other hand, the absence of Pauli limiting is expected for a triplet superconductor with equal-spin pairing state [170]. This is confirmed by the study of $B_{c2}(T)$ of single-crystalline UCoGe, see Section 7.3.3.

7.2.8. Discussion

Coexistence of ferromagnetism and superconductivity

The experimental results obtained on the polycrystalline samples prove that FM and SC coexist in UCoGe at ambient pressure. The magnetization data demonstrate UCoGe is a weak itinerant ferromagnet with a Curie temperature T_C = 3 K and a small ordered moment $m_0 = 0.03\ \mu_B$. The FM transition is furthermore corroborated by a weak maximum in the ac-susceptibility $\chi'_{ac}(T)$, a broad hump in the resistivity $\rho(T)$ and a small peak in the specific heat $c(T)$ near 3 K. The bulk character of ferromagnetism is provided by the large size of the negative peak in the linear coefficient of thermal expansion $\alpha(T)$ at T_C [171] (see Fig. 7.12) and the spontaneous muon precession frequency ν observed in the whole sample volume (see Fig. 7.10) below 3 K. Upon lowering temperature, superconductivity occurs. The resistive onset temperature which depends on the quality of samples reaches a value of 0.8 K for the best sample. Proof for bulk SC is obtained by the broad peaks in the specific heat (see the left panel of Fig. 7.6) and in the thermal expansion (see Fig. 7.12).

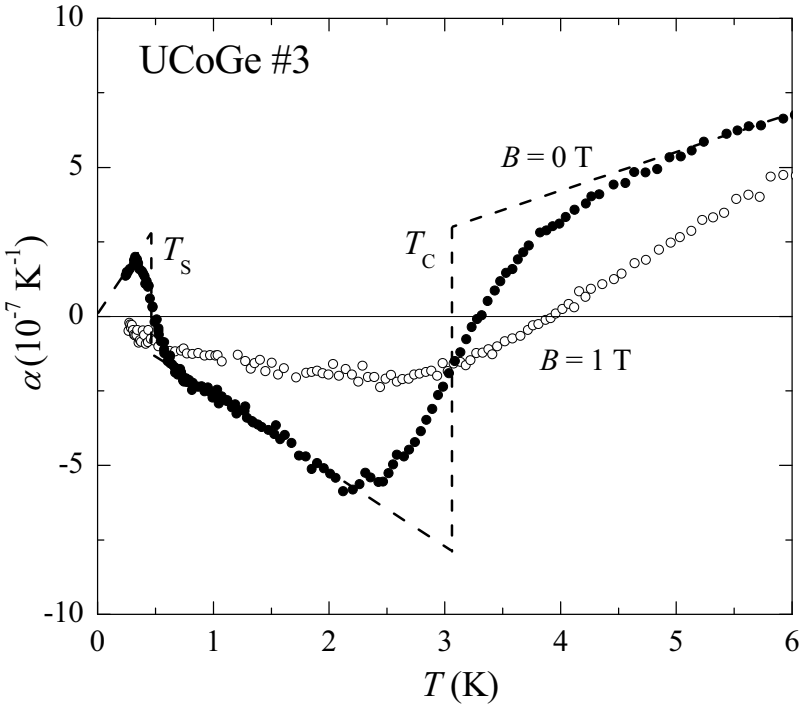

Figure 7.12 Temperature variation of the coefficient of the linear thermal expansion for UCoGe (sample #3) (data taken by A. Gasparini [171]). The large negative contribution below ~ 5 K is due to FM order. The dashed line gives the idealized transition in $\alpha(T)$ with $\Delta\alpha = -1.1\times10^{-6}$ K^{-1}. The total relative length change $\Delta L/L = (L(0.23\text{ K}) - L(T))/L$ associated with magnetic order is obtained by integrating $\alpha_{mag}(T)$ (*i.e.*, the difference between the experimental data and the linear term $\alpha = aT$ with $a = 1.1\times10^{-7}$ K^{-2} expected in the absence of FM order) and amounts to $+1.9\times10^{-6}$ K^{-1}. The peak below ~ 0.6 K is the thermodynamic signature of the SC transition. In a field of 1 T, applied along the dilatation direction $\Delta L/L$, the magnetic transition is smeared and SC is not resolved.

Co-existence of FM and SC is demonstrated by thermal expansion and μSR data. The total relative length change associated with SC, obtained by integrating $\alpha_S(T)$, amounts to $\Delta L/L = -0.1\times10^{-6}$ K^{-1} and is small compared to the length change $\Delta L/L = +1.9\times10^{-6}$ K^{-1}due to magnetic ordering (see caption of Fig. 7.12). Moreover, the spontaneous muon precession frequency associated with an internal field of ~ 200 G at the muon localization site is still observed at temperatures below T_S. This proofs that magnetism is not expelled below T_S and coexists with SC.

Proximity to a ferromagnetic quantum critical point

In addition to the small ordered moment and low Curie temperature, the $T^{5/3}$ temperature dependence of the resistivity for $T > T_C$ locates UCoGe close to the ferromagnetic instability (*i.e.* the limit $T_C \rightarrow 0$ K), in accordance with the SCR theory. The proximity to

the ferromagnetic critical point can be further investigated using the Ehrenfest relation for second order phase transitions $dT_C/dp = V_m T_C^{-1} \Delta\alpha/\Delta c$ (with the molar volume $V_m = 3.13\times10^{-5}$ m^3/mol). From the estimated step size in the thermal expansion and specific heat at T_C we calculate dT_C/dp = -0.25 K/kbar. This shows that the critical pressure p_c at which magnetism vanishes is low (an upper-bound for p_c assuming a linear suppression of T_C is ~ 12 kbar). In the same way we find that the superconducting transition temperature increases with pressure at a rate $dT_S/dp \approx 0.023$ K/kbar. In the scenario of the coexistence of *p*-state superconductivity and ferromagnetism [105], the increase of T_S with pressure places UCoGe in the phase diagram on the far side of the maximum in the superconducting dome with respect to the critical point (see Fig. 7.13). Accordingly, upon applying pressure, T_S is predicted to pass through a maximum before vanishing at the magnetic critical point. The derived pressure dependences of T_C and T_S for UCoGe have an opposite sign compared to the measured values for URhGe. In URhGe T_C shows a monotonic increase under pressures up to 120 kbar [120], and T_S is suppressed with pressure. The positive pressure dependence of T_S in UCoGe may explain the large difference in onset temperatures for superconductivity in the transport and bulk properties. Positive stress at the grain boundaries could cause a small volume fraction of the samples to have a larger T_S.

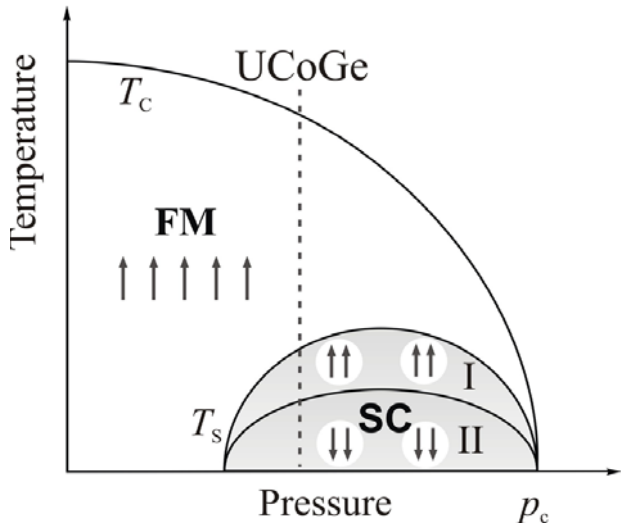

Figure 7.13 Schematic phase diagram in the temperature-pressure plane for a ferromagnetic superconductor. Two superconducting phases (grey) with up-spin pairing (I) and down-spin pairing (II) are contained in the ferromagnetic phase. Superconductivity and ferromagnetism coexist. After Ref.[107].

On the other hand, the difference of a factor of 7 in the size of the ordered moment m_0 (for URhGe the powder-averaged moment $m_0 = 0.21\ \mu_B$ [36]) and the opposite pressure effects

on T_C and T_S seem to indicate that UCoGe and URhGe represent two different cases of magnetically mediated SC. Indeed the recent observation of field-induced SC [38] in URhGe was taken as evidence for SC stimulated by a spin rotation in the neighborhood of a quantum phase transition under high magnetic field. In the case of UGe_2 the situation is again different as the FM to paramagnetic transition at the critical pressure becomes first order [34]. Moreover, evidence [86,110] is available that SC is driven by a changing Fermi surface topology associated with a metamagnetic jump in the magnetization. Consequently, unlike URhGe and UGe_2, UCoGe may present a genuine case of SC at a FM quantum critical point.

Following the publication of our discovery that UCoGe is a new ambient pressure ferromagnetic superconductor [171], several groups have initiated research on UCoGe. Two groups [172,173] confirmed the coexistence of ferromagnetism and superconductivity in polycrystalline samples. A detailed Co nuclear magnetic resonance and nuclear quadrupole resonance study on a powdered sample was carried out by Ohta *et al*. [172]. Knight shift measurements and the nuclear spin relaxation rate $1/T_1$ confirmed ferromagnetic fluctuations which possess a quantum critical character above T_C = 2.5 K. The onset of superconductivity was identified at 0.7 K, below which $1/T_1$ starts to decrease in 30 % of the volume fraction due to the opening of the superconducting gap.

Recently, also electronic structure calculations for UCoGe have been performed. De La Mora and Navarro [174] used a Linearized Augmented Plane Wave method based on the Density Functional Theory, where the strong correlations in uranium where included via the Local Density Approximation with a Hubbard term (LDA+U_H). The band structure calculations result in large localized moments on the U and Co sites. For the ferromagnetic calculation the U moment (1.7 μ_B) and the Co moment (-0.65 μ_B) are antiparallel and a net moment of ~ 1 μ_B results. This moment is much larger than the experimentally observed moment (0.03 μ_B). However, the authors argue that a non-collinear antiferromagnetic spin-arrangement of the uranium moment, resulting from the Dzyaloshinskii-Moriya interaction, gives rise to a weak ferromagnetic moment. Diviš [175] used a relativistic full-potential Augmented Plane Wave plus local orbitals method and the full-potential local-orbitals method. A stable ferromagnetic ground state was obtained, with a small uranium moment of 0.1 μ_B as a result of an almost complete cancellation between the spin (1.2 μ_B) magnetic moment and the antiparallel orbital (-1.1 μ_B) magnetic moment. However, also a small

moment of 0.2-0.4 μ_B was obtained at the Co site. Diviš argues that the small ferromagnetic moment of UCoGe could result from the antiparallel arrangement of the U and Co moments. This would imply however, a complex magnetic structure, for which experimental evidence is lacking. The DOS at the Fermi level is mainly due to the hybridization between the Co-3*d* and U-5*f* states and results in a specific-heat γ-value of 0.0127 J/molK^2, which is almost a factor 5 smaller than the experimental value. The exchange splitting amounts to 0.109 eV.

7.3. Single crystalline UCoGe

7.3.1. Sample preparation and characterization

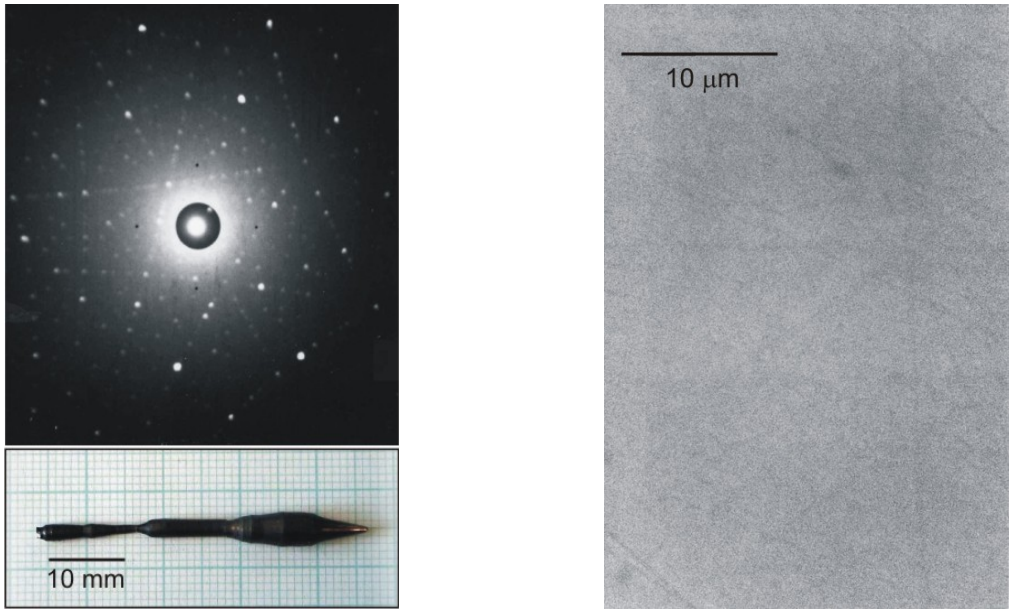

Figure 7.14 Left panel: X-ray Laue picture (*top*) of as-grown single crystalline UCoGe (*bottom*). *Right panel*: EPMA micrograph of the as-grown single crystal, which shows the single-phase nature U:Co:Ge 1:1:1.

A polycrystalline batch with nominal composition $U_{1.01}CoGe$ was prepared by arc melting the constituents (natural U 3N, Co 3N and Ge 5N) in a water-cooled copper crucible under a high-purity argon atmosphere. Next, a single-crystalline rod was pulled from the melt using a modified Czochralski technique in a tri-arc furnace under a high-purity argon atmosphere. Fig. 7.14 shows the as-grown single-crystal, which is 4 - 5 mm in diameter and 40 mm in length. EPMA analysis confirmed the single-phase nature of the grown crystal. The measured composition is $U_{0.9886}Co_{1.0124}Ge_{0.9971}$ within an experimental error of ± 0.015. Single-crystallinity was checked by X-ray Laue backscattering. Samples for various

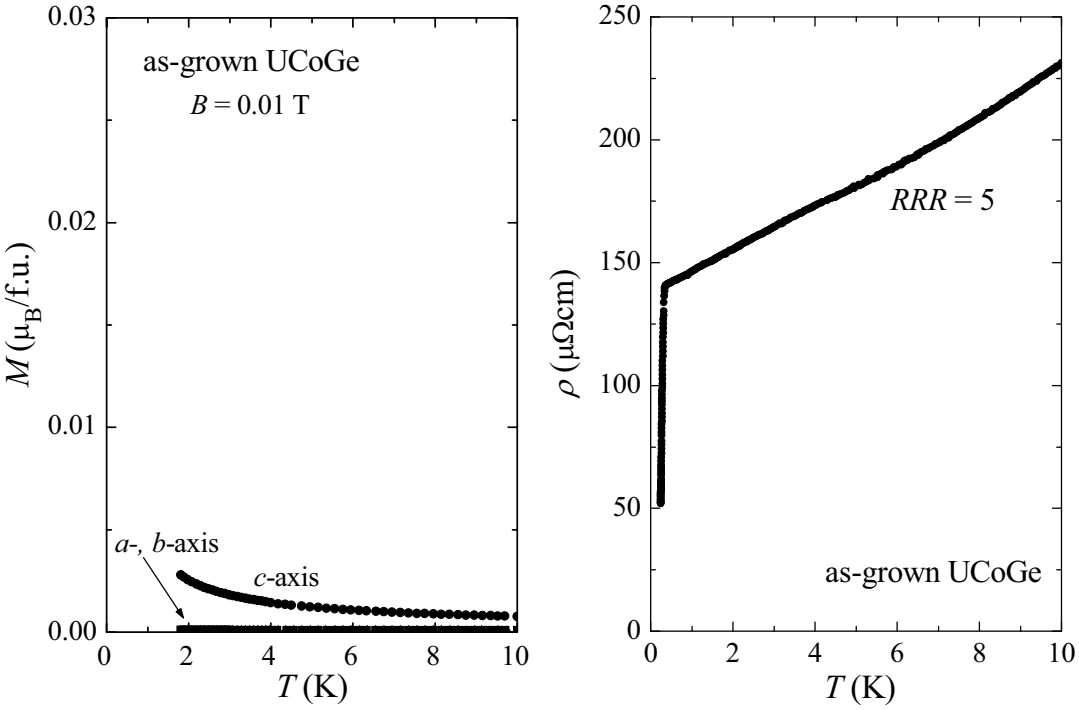

Figure 7.15 Left panel: Magnetization as a function of temperature in a field B of 0.01 T applied along the principal axes of as-grown single-crystalline UCoGe as indicated. *Right panel*: Temperature dependence of the electrical resistivity measured on as-grown single-crystalline UCoGe with $RRR \simeq 5$. (As the crystal was not oriented the direction of the current is not specified).

measurements were cut by spark erosion.

The temperature dependence of the resistivity and the magnetization of the as-grown single-crystal of UCoGe are represented in Fig. 7.15. The data show the sample has poor ferromagnetic and SC properties compared to polycrystalline UCoGe sample. The $RRR \simeq 5$. Superconductivity is observed below an onset temperature of 0.33 K, while the hump associated to FM transition in $\rho(T)$ is very weak. The magnetization data suggest the sample may undergo a magnetic transition with a Curie temperature below 2 K. The M(2K) values obtained for the as-grown single-crystal are lower than those obtained for the polycrystalline samples. Clearly, disorder suppresses FM and SC.

However, we succeeded in significantly improving the sample quality by an annealing procedure. Small pieces cut by spark-erosion were wrapped in tantalum foil and annealed in an evacuated quartz tube for one day at 1250 ^{o}C and 21 days at 880 ^{o}C. A similar annealing procedure was applied to URhGe [41]. EPMA analysis shows that the annealed pieces are homogenous and the single-phase nature remains with composition $U_{0.9752}Co_{1.0178}Ge_{1.0069}$ within the error of ± 0.015. Resistivity measurements on the annealed samples show that

the *RRR* increases to 30 and proper FM and SC transitions appear at 2.8 K and 0.6 K, respectively (see Fig. 7.16). These transition temperatures are in good agreement with those obtained for the best polycrystalline samples. The data reported in the remainder of this chapter are all taken on annealed single-crystalline UCoGe.

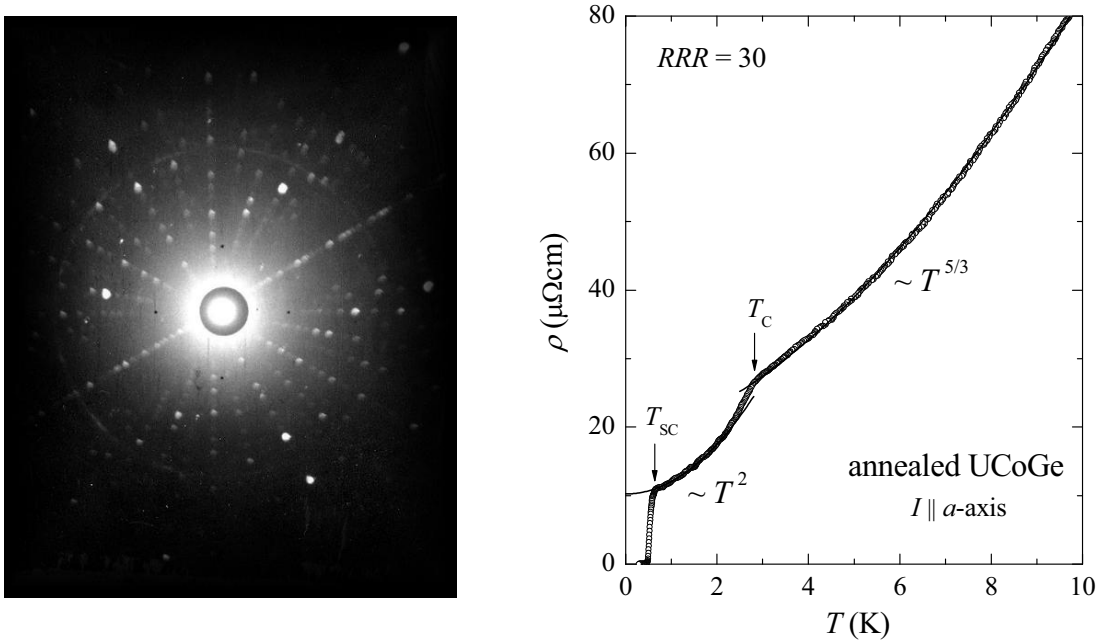

Figure 7.16 Left panel: X-ray Laue pattern of annealed single-crystalline UCoGe taken along the *c*-axis. *Right panel*: Temperature variation of the resistivity of annealed single-crystalline UCoGe for a current $I \parallel a$. Arrows indicate the Curie temperature T_C = 2.8 K and the onset temperature for the superconducting transition $T_{S,onset}$ = 0.6 K. The solid lines represent fits of the data to $\rho \sim T^2$ and $\sim T^{5/3}$ for the temperature ranges below and above T_C, respectively. The residual resistivity ρ_0 = 10.2 μΩcm and *RRR* = 30.

7.3.2. Magnetic properties

The temperature dependence of the magnetization $M(T)$ of single-crystalline UCoGe measured in a field of 0.01 T applied along the principal crystallographic axes is shown in Fig. 7.17. The T_C = 2.8 K is given by the inflection point in $M(T)$ for $B \parallel c$ or the temperature at which $dM(T)/dT$ has a minimum measured along the principal axes. T_C determined in this way agrees well with T_C deduced from the Arrott plots (see Fig. 7.18) and the location of the sharp kink in the resistivity curve (see Fig. 7.16). The magnetization curve for $B \parallel c$ $M(T)$ is well fitted to the relation $M(T)^2 = M_0^2(1 - (T/T^*)^2)$, as predicted for weak itinerant ferromagnets [176], with $T^* \sim T_C$ and the ordered moment $M_0 = 0.06\ \mu_B$/f.u.

Fig. 7.19 displays the field dependence of the magnetization $M(B)$ of single-crystalline

UCoGe measured in fields up to 5 T along the *a*, *b* and *c* axis at a temperature of 2 K. In accordance with $M(T)$, the anisotropy in the data shows that UCoGe is an uniaxial FM with

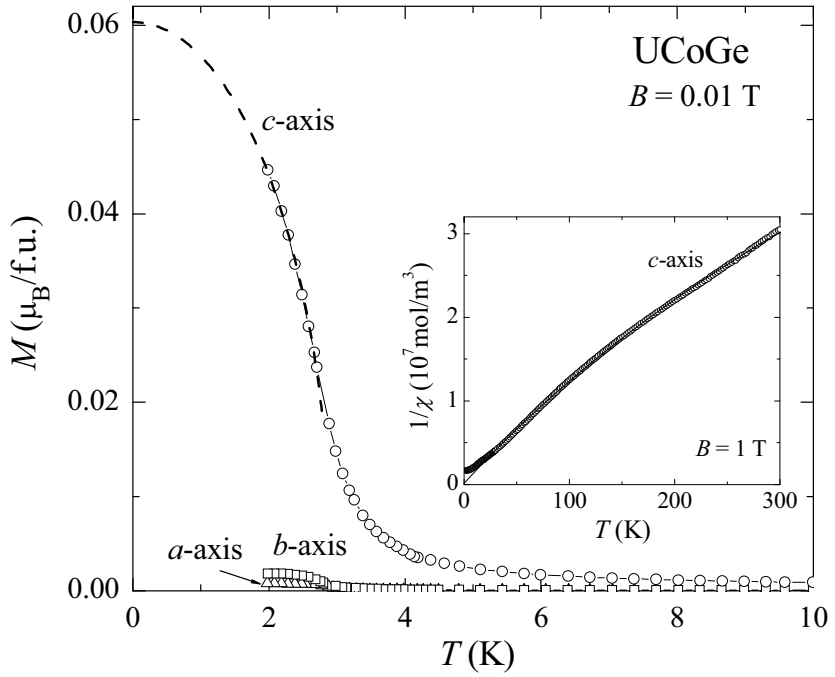

Figure 7.17 Magnetization as a function of temperature in a field B of 0.01 T applied along the principal axes of annealed UCoGe as indicated. The dashed line presents the fit to the relation $M(T)^2 = M_0^2(1 - (T/T^*)^2)$ (see text). *Inset*: Temperature variation of the reciprocal susceptibility of UCoGe single-crystal measured in a field of 1 T. The solid line is the best fit to a MCW law in the temperature range 50 - 300 K.

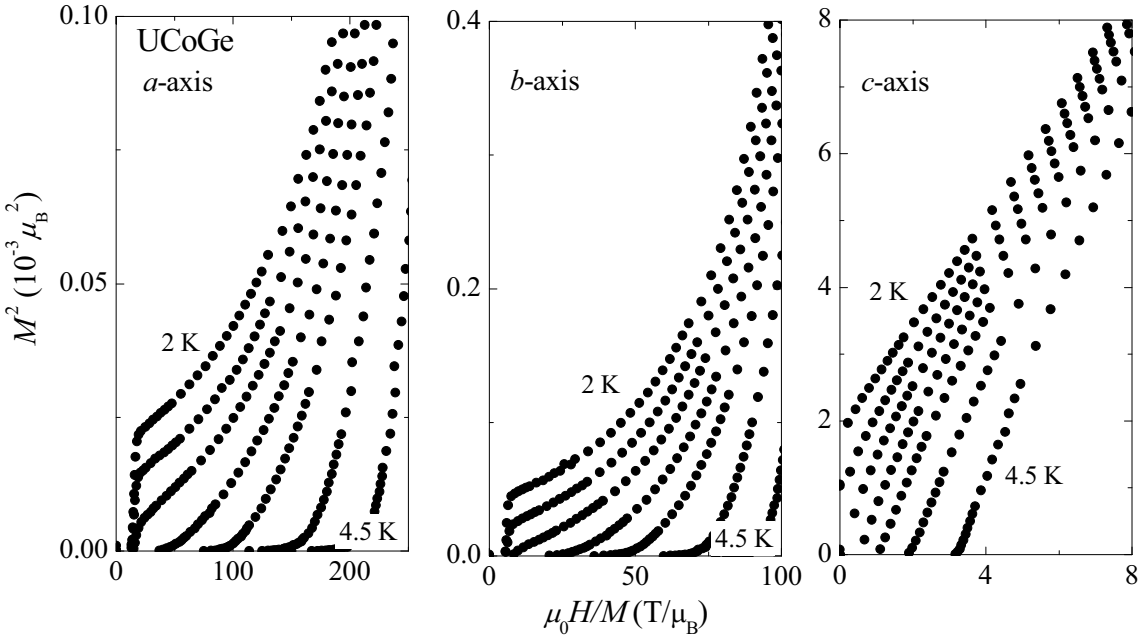

Figure 7.18 Arrott plots of the magnetization of single-crystalline UCoGe with the isotherms measured (from top to down) at T = 2, 2.4, 2.7, 3.0, 3.3, 3.8 and 4.5 K. The isotherm through the origin determines T_C = 2.8 K. Notice the different horizontal and vertical scales.

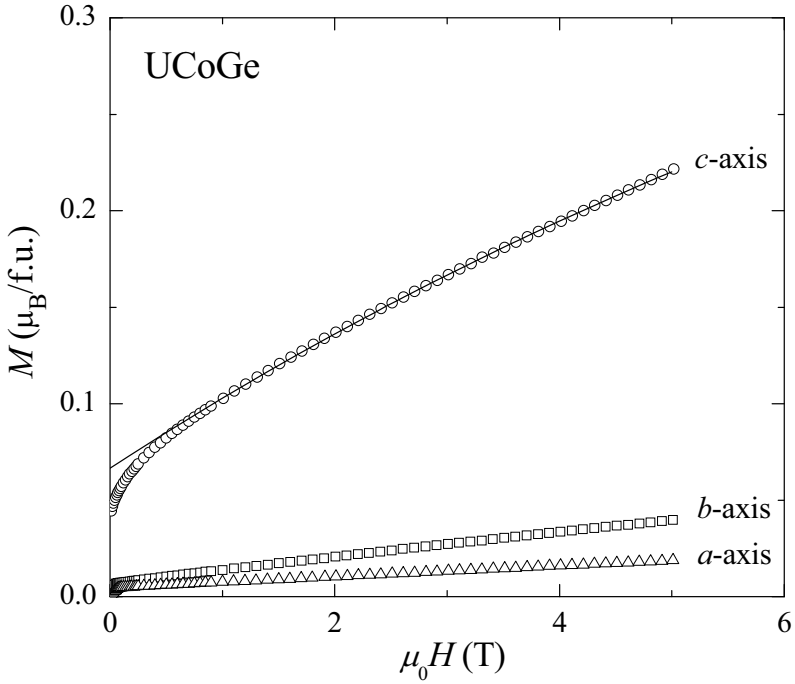

Figure 7.19 Field dependence of the magnetization of single crystalline UCoGe measured in a field up to 5 T along the *a*, *b* and *c* axis at 2 K. The solid line for $B \parallel c$ represents a fit to Eq. 4.3.

the ordered moment pointing along the *c* axis. By fitting the $M(B)$ curve for $B \parallel c$ to the empirical exponential function Eq. 4.3, the spontaneous magnetic moment is estimated at $M_S \simeq 0.07\ \mu_B$/f.u. This value is in agreement with the value $M_0 = 0.06\ \mu_B$/f.u obtained from $M(T)$ for $B \parallel c$ and the powder averaged value $M_{S,powder} = 0.03\ \mu_B$/f.u. $\simeq \frac{1}{2} M_{S,c\text{-axis}}$ (see Table 6.3). For $B \parallel a$, *b* the induced magnetization is small. The large initial increase in $M(B)$ for $B \parallel c$ is related to the relatively high temperature of $0.7T_C$ at which the data are taken.

The reciprocal susceptibility of the UCoGe single-crystal measured in a field $B = 1$ T along the *c*-axis in the temperature range 2 - 300 K is shown in the inset of Fig. 7.17. The magnetic susceptibility fitted to a MCW law in the temperature range 50 - 300 K yields $\chi_0 \sim 10^{-8}$ m^3/mol, an effective moment $p_{eff} = 2.15\ \mu_B$/f.u. and a small paramagnetic Curie temperature $\theta \approx -1$ K.

7.3.3. Unusual upper critical field B_{c2}

The suppression of superconductivity was investigated by resistivity measurements for a current along the *a*-axis in fixed magnetic fields applied along the orthorhombic *a* (longitudinal configuration), and *b* and *c* axis (transverse configuration), as shown in Fig. 7.20. Superconductivity appears below the onset temperature of 0.6 K. The SC

transition width $\Delta T_S \simeq 0.1$ K. The temperature at which SC is suppressed, T_S, is taken by the mid-points of the transitions. In a field ΔT_S gradually increases to 0.15 K at the highest fields (5 T). In an applied field the FM state rapidly forms a mono domain ($B < 0.01$ T) and we did not observe any hysteric behavior in B_{c2}. The main results are shown in Fig. 7.21. At least three remarkable features appear in the data:

(i) the large value of $B_{c2}(0) \approx 5$ T for $B \parallel a, b$

(ii) the large anisotropy, $B_{c2,\parallel a} \simeq B_{c2,\parallel b} \gg B_{c2,\parallel c}$, of a factor ~ 10

(iii) for all B-directions $B_{c2}(T)$ has a pronounced upturn when lowering the temperature.

Clearly, this behavior is at odds with standard BCS spin-singlet pairing.

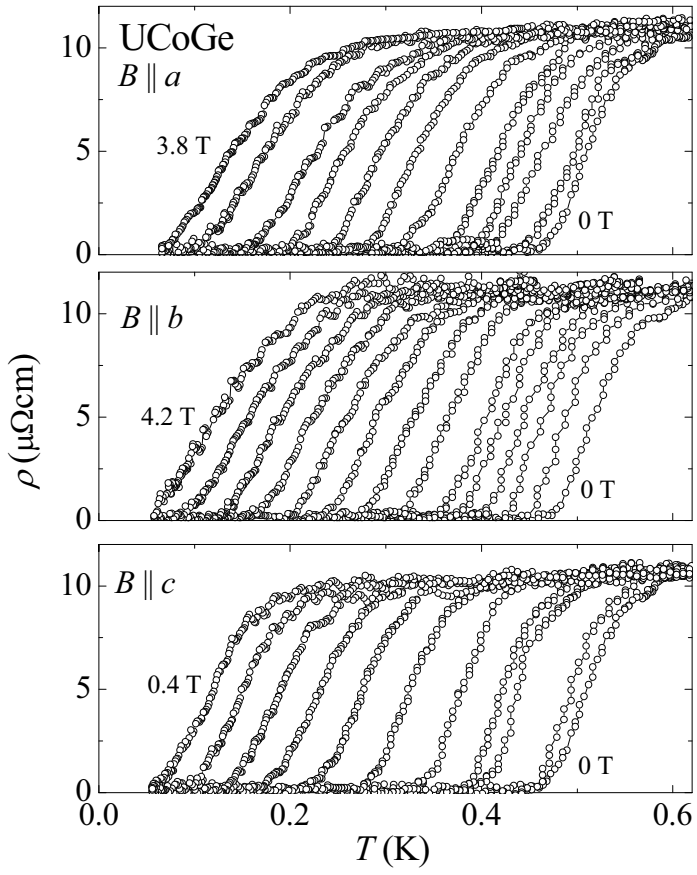

Figure 7.20 Temperature variation of the resistivity of single-crystalline UCoGe for a current $I \parallel a$ in various magnetic fields $B \parallel a$, b, and c.

Let us first address the large $B_{c2,\parallel a,b}(0)$. The Pauli paramagnetic limit for a weak coupling spin-singlet superconductor is $B_{c2,\mathrm{Pauli}}(0) = 1.83 T_S$ [169]. By including the effect of spin-orbit coupling a comparable $B_{c2}(0)$ value [177] results. Combined Pauli and orbital limiting could therefore in principle account for the small value $B_{c2,\parallel c}(0)$, but not for the large $B_{c2,\parallel a,b}(0)$ values. Also a strong-coupling scenario is unrealistic as this would involve a huge

coupling constant $\lambda \approx 20$ [178]. The absence of Pauli limiting for $B \parallel a,b$ therefore points to a triplet SC state with equal-spin pairing (ESP). A prerequisite for triplet pairing is a sufficiently clean sample, *i.e.* a mean free path ℓ larger than the coherence length ξ [168]. An estimate for ℓ and ξ can be extracted from the (large) initial slope $B_{c2,\parallel a,b}/dT$ = -7.9 and -8.4 T/K by using Eq. 7.6 and Eq. 7.7. With the specific heat coefficient $\gamma = 1.82 \times 10^3$ J/K^{2}m^3 and $\rho_0 = 10.2 \times 10^{-8}$ Ωm we calculate $\ell \approx 900$ Å and $\xi \approx 120$ Å and conclude our single crystal satisfies the clean-limit condition. Notice that for $B \parallel c$, B'_{c2} attains the low value 0.7 T/K, and Eq. 7.5 does not yield proper results.

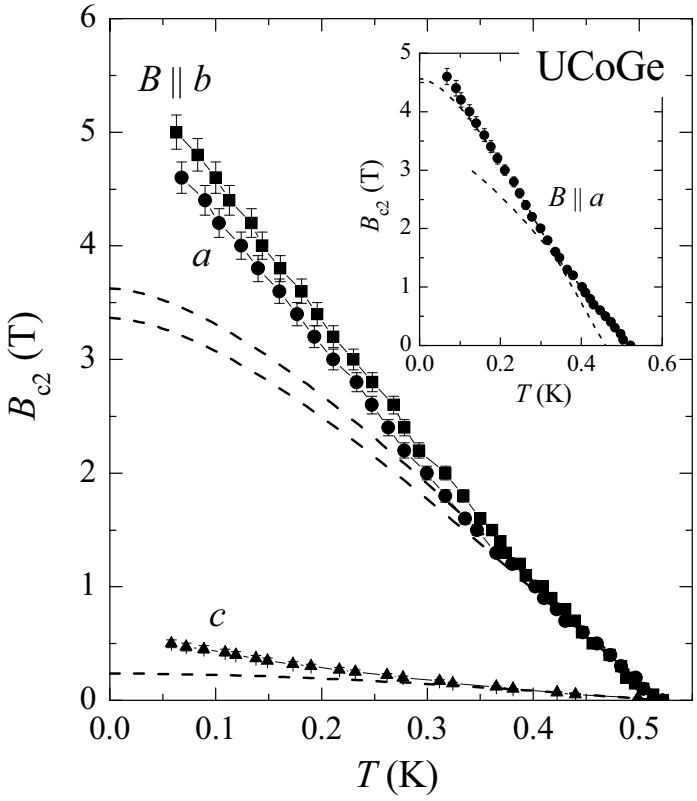

Figure 7.21 Temperature dependence of the upper critical field of UCoGe for B along the principal axes. The dashed lines show the calculated dependence for a superconducting gap function with axial (along c axis) and polar symmetries (along a and b axis) (see text). *Inset*: $B_{c2}(T)$ for $B \parallel a$, plotted together with the polar state functions for two superconducting phases with zero-field transitions at 0.46 and 0.52 K.

The order parameter in an orthorhombic itinerant ferromagnetic superconductor with spin-triplet pairing and strong spin-orbit coupling has been worked out by Fomin [111] and Mineev [112]. Under the assumption that the exchange splitting of the Fermi surface is sufficiently large, such that the pairing between electrons from spin-up and down bands is negligible, equal-spin pairing will give rise to two-band superconductivity with gap

functions $\Delta_{\uparrow\uparrow}(R,k) = -\eta_1(R)f_-(k)$ and $\Delta_{\downarrow\downarrow}(R,k) = \eta_2(R)f_+(k)$, where $\eta_{1,2}$ are the order parameter amplitudes. From the symmetry-group analysis for an orthorhombic uniaxial FM it follows that only two SC gap-structures $f_\pm(k)$ are possible. Assuming that the ordered moment m_0 is directed along the z axis, then the SC gap has zeros (nodes) parallel to the magnetic axis ($k_x = k_y = 0$, *A* phase) or a line of zeros on the equator of the Fermi surface ($k_z = 0$, *B* phase). In other words, the *A* phase has a gap function of axial symmetry with nodes along m_0 and the *B* phase has a gap of polar symmetry with a line of nodes perpendicular to m_0.

Table 7.1 Parameters of the normal and of the superconducting state of (annealed) single-crystalline UCoGe. The residual resisitvity ρ_0 = 10.2 μΩcm and the superconducting transition temperature T_S = 0.52 K are obtained in zero-field.

Parameter		Units	$B \parallel a$	$B \parallel b$
B'_{c2}	slope of $B_{c2}(T)$ at T_S	T/K	7.9	8.4
S_S	effective Fermi surface	10^{20} m^{-2}	1.75	1.69
m^*	effective mass	m_e	94	96
υ_F	Fermi velocity	m/s	4611	4455
ξ	BCS-coherence length	10^{-8} m	1.22	1.18
ℓ	total mean free path	10^{-8} m	8.76	9.07
λ_L	London penetration depth	10^{-8} m	123	127
GL	Ginzburg-Landau parameter	-	98	104

The effect of an anisotropic *p*-wave interaction on B_{c2} has been investigated by Scharnberg and Klemm [179]. For a *p*-wave interaction that favors one direction over the other two, a polar state has the highest T_S, while conversely, if the *p*-wave interaction is weakest in one direction an axial state is favored. Since the SC gap is fixed to the crystal lattice by spin-orbit coupling, B_{c2} in general will show a strong anisotropy. We first consider the case of a polar state with the maximum gap direction along the uniaxial direction $m_0 \parallel c$ (*i.e.* the strength of the pairing interaction along c is stronger than in the ab plane, $V_c > V_{ab}$). The upper critical fields have been calculated for B in the plane of the nodes ($B \perp m_0$) (CBS = Completely Broken Symmetry state) and $B \parallel m_0$ along the maximum of the gap (polar state) [179]. For $V_{ab} = 0$ their ratio for $T \rightarrow 0$ is given by $B_{c2,\perp}(0)/B_{c2,\parallel}(0) = 0.466(m_{ab}/m_c)^{1/2}$, where m_{ab}/m_c reflects the anisotropy in the effective mass. For our orthorhombic material m_{ab}/m_c is of the order of 1 and the model predicts $B_{c2,\perp}(0)/B_{c2,\parallel}(0)$ is ~ 1/2. This is at

variance with the results in Fig. 7.21 where the anisotropy ratio ~ 10 and we conclude that a polar gap cannot explain the anisotropy in B_{c2}. For the axial state (nodes along $m_0 \parallel c$ and the maximum gap in the *ab* plane) the anisotropy in B_{c2} is reversed [179] $B_{c2,\perp}(0) > B_{c2,\parallel}(0)$. This is the situation in UCoGe. $B_{c2,\parallel}(T)$ has been calculated in Ref. [180] (Anderson-Brinkman-Morel (ABM) state), but calculations for $B_{c2,\perp}(T)$ are not at hand. However, since the gap is maximum one may assume that $B_{c2,\perp}(T)$ can be represented by the polar function. In Fig. 7.21 we compare the anisotropy in B_{c2} calculated in this way, with the experimental results. We conclude that the measured anisotropy supports an axial state, but the model calculations do not track the experimental results at lower *T*. This is due to the pronounced positive curvature in $B_{c2}(T)$, which we discuss next.

For $B \parallel a$ and *b* the slope $-\mathrm{d}B_{c2}/\mathrm{d}T$ has initial values of 7.9 and 8.4 T/K but increases to 11.4 and 12.1 T/K at lower *T*. For $B \parallel a$ the increase is rather abrupt (kink-like) and takes place in a narrow *T* range centered around 0.33 K (see inset in Fig. 7.21), while for $B \parallel b$ the increase is more gradual. An overall smooth increase of B_{c2} is observed for $B \parallel c$. We stress that if we define T_S in another way, like by $T_{S,onset}$ or by the 10% or 90 % points (measured by the drop in resistance) the absolute values for B_{c2} change slightly, but the upward curvature remains. An upward curvature in $B_{c2}(T)$ was also reported for the polycrystalline samples (see Section 7.2.7).

Several appealing explanations for a kink ($B \parallel a$) or upward curvature ($B \parallel b$) in $B_{c2}(T)$ have been given in the literature, of which a cross-over between two phases in a two-band ferromagnetic superconductor [106] is perhaps the most interesting. Mineev and Champel [106] have evaluated the linearized Ginzburg-Landau equations including gradient terms for a cubic two-band FM superconductor with gaps $\Delta_{\uparrow\uparrow}$ and $\Delta_{\downarrow\downarrow}$. Depending on the strength of the pairing interactions measured by $g_1 = V_{\uparrow\uparrow}\langle|f_-(k)|^2 N_{0\uparrow}(k)\rangle$ and $g_2 = V_{\downarrow\downarrow}\langle|f_+(k)|^2 N_{0\downarrow}(k)\rangle$ (here $N_{0\uparrow,\downarrow}$ is the angular dependent density of states) and a number of anisotropy coefficients, an upturn in $B_{c2}(T)$ is predicted. In the more anisotropic situation of an orthorhombic system, calculations are more tedious, but also then a cross-over between ESP states in field is possible. Notice that in the two-band model it is not a priori known what the ground state is ($|\uparrow\uparrow\rangle$ or $|\downarrow\downarrow\rangle$), as this depends on g_1 and g_2 and the anisotropy coefficients.

In order to illustrate the possibility of the two-band superconductivity scenario we have plotted in the inset in Fig. 7.21 the polar state functions [180] for two SC phases with zero-field transition temperatures of 0.46 and 0.52 K. A description with two polar gaps tracks the experimental data down to $T \simeq 0.16$ K, but fails there below. Note however that in the two-band model of Ref. [106] only one superconducting transition appears in zero-field, as the second phase is induced by the magnetic field. Bulk measurements, like specific heat, to probe the superconducting transition of our single crystals, have not been performed yet. Another interesting scenario for an upwards curvature in B_{c2} is a rotation of the quantization axis of the ESP state from along m_0 at low fields, towards the field direction in high fields. The upward curvature in $B_{c2,\| c}$ is then possibly explained by the field not being perfectly aligned along c. Scharnberg and Klemm [179] have also investigated the possibility of a kink in B_{c2}. For the axial symmetric case a kink appears for $B \| c$ for a specific ratio of the strength of the pairing interaction, namely $V_c/V_{ab} < 0.866$, which could give rise to a transition from the Scharnberg-Klemm state to the polar state. However, an upturn is not predicted for B directed in the ab plane. The only other unconventional superconductor which shows a clear kink in B_{c2} is the heavy-fermion material UPt_3 [181]. Here the kink is attributed to the intersection of two $B_{c2}(T)$ curves of the two SC phases [182] even in the absence of a magnetic field. The split transition is attributed to the coupling of a two-component order parameter, belonging to the E_{1g} or E_{2u} representation in the hexagonal crystal, to a symmetry breaking field.

7.3.4. Discussion

The occurrence of SC in a FM material is naturally explained [105] by the formation of Cooper pairs with parallel spin. Within the symmetry classification for orthorhombic itinerant FM spin-triplet superconductors [106] the SC gap is predicted to be anisotropic with point nodes along the magnetic moment direction or line nodes in the plane perpendicular to the moments.

In UCoGe the proximity to the magnetic instability, the defect sensitivity of T_S, and the absence of Pauli limiting are all in agreement with such a scenario. The study of the upper critical field of single-crystalline UCoGe results in an axial SC gap with nodes along the moment direction.

In the case of FM superconductor URhGe, which belongs to the same symmetry class as

UCoGe, the upper critical field has been investigated by Hardy and Huxley [41]. B_{c2}, measured on single-crystals with *RRR*'s of 21 and 34, *i.e.* comparable to the value of the UCoGe single crystal, also show a large anisotropy. The data do not show any sign of an upward curvature and are well described by the model functions for a polar state with a maximum gap parallel to *a*, and for the CBS state [179] with nodes in the direction of *b* and *c*. This polar gap structure takes into account the easy-(*bc*)-plane nature of the magnetization: $m_0 = 0.42\ \mu_B$ points along *c*, but for $B \parallel b$ rotates towards the *b* axis [38]. Surprisingly, superconductivity reappears when the component of the applied field along the *b* axis reaches ~ 12 T [38] and the ordered moment rotates towards the *b* axis. Compelling evidence is at hand that in the high-field as well as in the low-field SC phase, superconductivity is stimulated by critical magnetic fluctuations associated with the field-induced spin- reorientation process. Near the quantum critical point an acute enhancement of B_{c2} is observed [104] and superconductivity survives in fields as large as 28 T applied along *a*. It will be highly interesting to investigate whether the apparent lack of saturation of B_{c2} for $T \rightarrow 0$ in UCoGe has a similar origin, namely the proximity to a field-induced quantum critical point.

7.4. Conclusion

In conclusion, we have discovered a new member of the family of ferromagnetic superconductors: UCoGe. Measurements of the magnetic, transport and thermal properties on polycrystalline samples provide solid evidence for bulk superconductivity below 0.6 K, which coexists with bulk weak itinerant ferromagnetism with a Curie temperature of 3 K. Magnetization measurements on single-crystalline samples show that UCoGe is a uniaxial ferromagnet with the ordered moment $m_0 = 0.06\ \mu_B$ directed along the orthorhombic *c*-axis. Transport measurements were used to determine the magnitude and anisotropy of the upper critical field B_{c2}. The upper critical field data support unconventional *p*-wave superconductivity and point to an axial SC gap function with nodes along the moment direction m_0. The pronounced upward curvature ($B \parallel b$) or kink ($B \parallel a$) observed in the B_{c2} curves suggests UCoGe is a two-band ferromagnetic superconductor [105-107].

Since SC occurs right on the borderline of FM order at ambient pressure, UCoGe offers a unique testing ground to investigate the long-standing issue of SC stimulated by critical spin-fluctuations associated with a magnetic quantum critical point.